Biomaterials 31 (2010) 7758–7765

Contents lists available at ScienceDirect

Biomaterials

journal homepage: www.elsevier.com/locate/biomaterials

The interaction between nanoscale surface features and mechanical loading and its effect on osteoblast-like cells behavior

Ljupcho Prodanov [a], Joost te Riet [b], Edwin Lamers [a], Maciej Domanski [c], Regina Luttge [c], Jack J.W.A. van Loon [d], John A. Jansen [a], X. Frank Walboomers [a,*]

[a] Radboud University Nijmegen Medical Centre, Department of Biomaterials, P.O. Box 9101, 6500HB Nijmegen, The Netherlands
[b] Nijmegen Centre for Molecular Life Sciences, Department of Tumor Immunology, Radboud University Nijmegen Medical Centre, Nijmegen, The Netherlands
[c] MESA+Institute for Nanotechnology, University of Twente, P.O. Box 217, 7500 AE Enschede, The Netherlands
[d] DESC @ OCB-ACTA, VU University, Amsterdam, The Netherlands

ARTICLE INFO

Article history:
Received 27 April 2010
Accepted 28 June 2010
Available online 20 July 2010

Keywords:
Nanotopography
Surface modification
Surface texture
Silicone elastomer
Bone remodeling

ABSTRACT

Osteoblasts respond to mechanical stimulation by changing morphology, gene expression and matrix mineralization. Introducing surface topography on biomaterials, independently of mechanical loading, has been reported to give similar effects. In the current study, using a nanotextured surface, and mechanical loading, we aimed to develop a multi-factorial model in which both parameters interact. Mechanical stimulation to osteoblast-like cells was applied by longitudinal stretch in parallel direction to the nanotexture (300 nm wide and 60 nm deep grooves), with frequency of 1 Hz and stretch magnitude varying from 1% to 8%. Scanning electron microscopy showed that osteoblast-like cells subjected to mechanical loading oriented perpendicularly to the stretch direction. When cultured on nanotextured surfaces, cells aligned parallel to the texture. However, the parallel cell direction to the nanotextured surface was lost and turned to perpendicular when parallel stretch to the nanotexture, greater than 3% was applied to the cells. This phenomenon could not be achieved when a texture with micro-sized dimensions was used. Moreover, a significant synergistic effect on upregulation of fibronectin and Cfba was observed when dual stimulation was used. These findings can lead to a development of new biomimetic materials that can guide morphogenesis in tissue repair and bone remodeling.

1. Introduction

Bones provide structural support to the body, organizing its components in space, protecting vital organs, and transmitting muscle forces from one part of the body to another. The buildup of the bone macro morphology, the internal orientation of the collagen filaments, as well as the individual bone cells are all adjusted in shape and orientation according to the principle load direction [1–5]. Mechanotransduction in bone is complex in nature, and influenced by many modulators such as muscular loads [6,7], fluid flow through the bone lacuna-canalicular system [8,9], gravity [10–12], compressive loading, and tensile stresses [13]. The mechanical stimulation applied to the cells in bone tissue is extremely important, as osteoblasts change cell morphology, proliferation, and differentiation [14–16].

The most studied proteins in osteoblast mechanobiology are the integrins. Upon stimulation, integrins act as mechanosensors and trigger intracellular signaling cascades [17], including MPAKs, Cox-2, NO, and TNF-alpha [18–20], which are downstream effectors of a wide range of transcription factors involved in cell survival and differentiation. In vitro under the influence of uniaxial stress, bone-like cells have the tendency to orient themselves perpendicular to the direction of stretch [21]. Such reorientation coincidents with an enhanced capacity of differentiation, and extracellular matrix (ECM) mineralization.

Independent of mechanical loading, the morphology of the culture substrate has been reported to have similar effects on bone cells. Microscale grooves have been shown to cause contact guidance and alignment parallel to the groove direction [22]. The effects of such substrate topographical structures have also been shown to affect gene expression and differentiation capacity [23–25]. Previous studies looking in the interaction between effects initiated from topography and loading showed that cells always retain their alignment on micropatterned substrate during cyclic uniaxial strain, independent of the stretch magnitude or whether the

* Corresponding author at: Radboud University Nijmegen Medical Centre, Department of Biomaterials, PO Box 9101, 6500HB Nijmegen, The Netherlands. Tel.: +31 243614086; fax: +31 243614657.
E-mail address: f.walboomers@dent.umcn.nl (X.F. Walboomers).

0142-9612/$ – see front matter © 2010 Elsevier Ltd. All rights reserved.
doi:10.1016/j.biomaterials.2010.06.050

microgrooves were oriented parallel or perpendicular to the stretching direction [26]. Cells primarily adjusted their shape according to the substrate texturing, which effectively overruled the role played by mechanical loading. This showed that micrometer-sized patterns are insufficient as a study model in this respect. Moreover, also from a physiological point of view micrometer-sized textures seem insufficient. The bone ECM is highly organized nanostructured mesh surrounding the cells [27]. Therefore it can be postulated that using nanotextured substrate will more closely resemble the in vivo environment and provide a new concept in the field of cells mechanics.

In the current study, our hypothesis was that using a nanotextured surface, and mechanical loading, for the first time, we can develop a multi-factorial model in which both parameters truly interact. The aim of this study was to design a multi-factorial system which will use nanotextured substrate and mechanical loading. Secondly, we hypothesised that such a dual stimulation will show synergistic effects on cell behavior in terms of cell attachment, ECM formation and osteoblast differentiation potential.

2. Materials and methods

2.1. Silicone rubber dishes

Silicone (polydimethylsiloxane, Elastosil RT 601; Wacker-Chemie, Germany) was casted into acryl dish molds and cured for 3 h at 50 °C. The resulting dishes with culturing surface of 1.5 × 3 cm^2, were further processed as-described in the next steps.

2.2. Preparation of nanotextured surfaces

Nanotextured groove patterns were made using laser interference lithography (LIL) and reactive ion etching techniques as-described by Walboomers et al. and Lamers et al. [28,29]. In this study, patterned wafers with 300 nm wide grooves (600 nm pitch) and depth of ~150 nm were used. To confirm previous results 1 μm wide, and 500 nm deep (pitch 2 μm), microtextured wafers were also prepared.

Using the method of solvent casting, the wafers were used to prepare polystyrene (PS) replicas as-described by van Delft [30]. Briefly, a casting solution was made by dissolving pieces from tissue culture polystyrene (Greiner, Kremsmünster, Austria) in chloroform (25 g/150 mL; Labscan, Dublin, Ireland) and stirring gently for 24 h. After casting this solution on the silicon wafer, the chloroform evaporated overnight in a laminar flow hood and the PS were removed in milli-Q water. After given a radio frequency glow discharge (RFGD) treatment (Harrick, USA) for 5 min at 100 mTorr Ar. These PS replicas were then used as a second template for production of the final silicone rubber patterned substrate. The same procedure as above was used to prepare the silicone patterned rubber. After curing, the silicone rubber replicas were removed from the template in milli-Q water as shown in Fig. 1(a). The obtained silicone patterned substrates were bonded to the bottoms of the silicone dishes described above, using room temperature vulcanizing silicone adhesive (Nusil Technology, Carpinteria, CA). The patterned substrates were always attached in parallel to the stretch direction. Smooth silicone substrates were prepared to serve as a control group. Before use, dishes were cleaned in a 10% Liquinox (Alconox Inc., White Plains, NY)/milli-Q solution, washed 10 times with milli-Q, rinsed with 100% EtOH, and autoclaved at 121 °C for 15 min. Before cell seeding, all experimental substrates received a RFGD treatment of 5 min at 100 mTorr to enhance substrate wettability and cell attachment, and left to attach overnight in the cell incubator. The next day cells were subjected to uniform, uniaxial, cyclic strain using a custom-made stretching apparatus as-described previously [26,31].

2.3. Surface analysis with atomic force microscopy (AFM)

Surface topography was quantitatively evaluated using atomic force microscopy (AFM; Dimension 3100, Veeco, Santa Barbara, CA). Tapping in ambient air was performed with 118 μm long silicon cantilevers (NW-AR5T-NCHR, NanoWorld AG, Wetzlar, Germany) with average nominal resonant frequencies of 317 kHz and average nominal spring constants of 30 N/m. This type of AFM probe has a high aspect ratio (7:1) tip with a nominal length of >2 μm and a half-cone angle of <5°. Nominal radius of curvature of the AFM probe tip was less than 10 nm. The probes are especially suited to characterize the manufactured nanogrooves. Height images of each field/sample were captured in ambient air at 50% humidity at a tapping frequency of 266.4 kHz. The analyzed field was scanned at a scan rate of 0.5 Hz and 512 scanning lines. Nanoscope imaging software (version 6.13r1, Veeco) was used to analyze the resulting images.

2.4. Cell culture

Rat bone marrow mesenchymal stem cells (MSCs) were isolated from femur of 40–43-day-old male Wistar rats based on the method described by Maniatopoulos et al. [32]. Briefly, MSCs were obtained by flushing out the marrow from two femurs with α-minimal essential medium (α-MEM) containing 2% gentamycin (all from Gibco BRL, Life Technologies BV, Breda, The Netherlands). The washout cells were cultured in three T-75 flasks in a humidified atmosphere of 95% air, 5% CO_2 at 37 °C with osteogenic medium containing α-MEM, 10% fetal calf serum (FCS), 10 mM sodium β-glycerophosphate, 10^{-8} M dexamethasone, 50 mg/mL ascorbic acid, and 50 mg/mL gentamycin (all Gibco).

The following day, the medium was refreshed to remove all non-adherent cells. After 6 days the adherent cells were trypsinized using trypsin/EDTA (0.25% w/v trypsin/0.02% EDTA), and counted with a Coulter® Counter (Coulter Electronics, Luton, UK).

2.5. Mechanical stimulation

To examine the interaction between the nanotextured surface and the mechanically stimulated environment on cell alignment, first a cell alignment study was performed. Cells were seeded at a density of 1 × 10^4 cells/cm^2. Different cyclic stretching magnitudes of 1, 2, 3, 4, 5, 6, 7 and 8% at a 1 Hz frequency with intermittent stretch duration (15 min stretch/15 min rest for 16 h, followed by 8 h of rest) were used for two days. Cells were cultured in four different conditions using: a) smooth surface, b) smooth surface subjected to stretch, c) nanotextured surface, and d) nanotextured surface subjected to stretch. The mechanical loading was applied by longitudinal stretch in parallel direction to the nanotexture as depicted in Fig. 1(b).

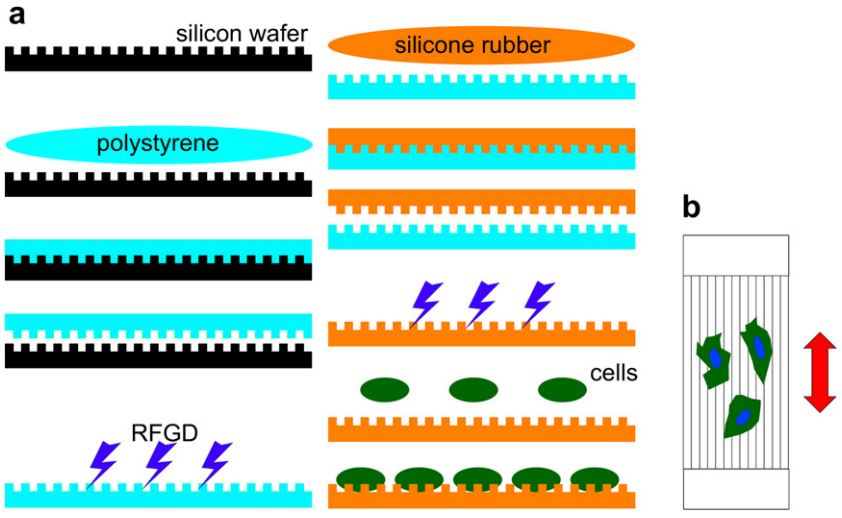

Fig. 1. Graph showing the casting procedure (a), longitudinal stretch in parallel direction to the nanotexture (b).

In all subsequent investigations the stretch magnitude was based on the cell alignment study, whereas the stretch frequency stayed unchanged.

2.6. Immunofluorescence and image analyses

To observe the cytoskeleton, cells were fixed for 10 min in 3% paraformaldehyde (Fluka AG), and permeabilized with 1% Triton X-100 (LTD Colebrook, Bucks, England) for 5 min. Then filamentous actin was stained with Alexa Fluor 568 phalloidin (Molecular Probes Inc., Eugene, OR) diluted 1:200 in PBS containing 1% Bovine Serum Albumin (BSA) for 2 h. The cell nucleus was stained with 4′,6-diamidino-2-phenylindole (DAPI) diluted in PBS 1:2500 for 10 min. Finally, the specimens were examined with an automated fluorescent Zeiss microscope (imager Z1), at magnification of 20×. For each sample, the microscopic fields were selected randomly (more than 100) and the actin filaments were examined for their overall orientation with respect to the groove and stretch direction using Image J software (Image J, La Jollia, USA). Only cells that were attached to the surface, not in contact with other cells, and not in contact with the image perimeter were measured. Then median angles and standard deviations were calculated using an unpaired *t*-test.

2.7. Scanning electron microscopy (SEM)

To assess cellular morphology and confirm cell realignment, SEM was used. Directly after stretching, cells were washed with phosphate buffered saline (PBS), fixed for 5 min in 2% glutaraldehyde, rinsed for 5 min with 0.1 M sodium-cacodylate buffer (pH 7.4) (Acros Organics), dehydrated in a graded series of ethanol and dried in tetramethylsilane (Acros Organics) to air. The specimens were sputtercoated with Pt and examined using SEM (JEOL 6330).

2.8. Isolation of RNA and reverse transcriptase PCR

Cells were seeded with a density of 3×10^4 cells/cm^2, three times the density as used for orientation studies in order to obtain a sufficient amount of RNA. Total RNA was extracted using the Trizol method immediately after the mechanical loading was stopped. Briefly, cells were washed with PBS before adding 1 mL of Trizol (Invitrogen). The cell extract was collected, mixed with 0.2 mL chloroform and centrifuged for 15 min at 12 000× g at 4 °C. Only the upper aqueous phase was collected and mixed with 0.5 mL isopropyl alcohol (Labscan, Dublin, Ireland). After 10 min of incubation on room temperature, the extract was centrifuged at 12 000× g for 10 min at 4 °C and washed 2× with 75% alcohol following centrifugation at not more than 7500× *g* for 5 min. The RNA pallet was dissolved in RNA free water and the total RNA concentration was measured with spectrophotometer (Biorad, Smart Spec Plus). The reverse transcriptase (RT) reaction was performed in three steps. In the first step 1 μg of total RNA in 13 μL of RNA free water, 1.15 μL 150 ng of random primers, and 1.15 μL dNTP mix (25 mM each) were incubated in PCR device (65 °C, 5 min) and quickly chilled on ice. In the second step 4.6 μL 5X First Strand Buffer (250 mM Tris–Cl, pH 8.3, 375 mM KCl, 15 mM $MgCl_2$) and 2 μL 0.1 M DDT were added (25 °C, 10 min) and finally in the third step 1.15 μL Superscript was added (50 min, 42 °C) (15 min, 70 °C) (all reagents from Invitrogen).

2.9. Real-time PCR

The gene expression on RNA level for genes involved in cell attachment (integrin α1, and integrin β1), formation of ECM (fibronectin, collagen type I), and osteoblasts differentiation (alkaline phosphatase (ALP), osteocalcin (OC), bone sialoprotein (BSP) and Cfba) were evaluated after 2 days of cell culture stimulation in four different conditions. The expression levels were analyzed versus the housekeeping gene glyceraldehydes 3-phosphate dehydrogenase (GAPDH). The forward and reverse primer sequence can be found in Table 1. Specific sense and antisense primers for the genes were designed according to published cDNA sequences of GenBank. The specificity of the primers was tested separately before the real-time PCR reaction. IQ SYBR Green Supermix PCR kit (BioRad, Hemel Hempstead, United Kingdom) was used for real-time measurement. Relative mRNA expression was quantified using the comparative Ct (DCt) method and expressed as 2^{-DDCt}. Each sample was done in duplicate and expressed as mean ± standard deviation. The RNA-negative control consisted of only milli-Q water that is reverse transcribed and amplified in parallel with the cell samples.

2.10. Statstical analyses

The complete experiment was performed three times. Every sample was measured in duplicate. Statistical analysis was performed using an unpaired *t*-test. Calculations were performed in InStat (v. 3.05 GraphPad Inc, San Diego, CA).

Table 1
Forward and reverse primer sequences.

	Forward (5′ → 3′)	Reverse (5′ → 3′)
Integrin α1	AGCTGGACATAGTCATCGTC	AGTTGTCATGCGATTCTCCG
Integrin β1	AATGTTTCAGTGCAGAGCC	TTGGGATGATGTCGGGAC
Collagen 1	AACCCGAGGTATGCTTGATCT	CCAGTTCTTCATTGCATTGC
Fibronectin	CCTTAAGCCTTCTGCTCTGG	CGGCAAAAGAAAGCAGAACT
Osteocalcin	CGGCCCTGAGTCTGACAAA	GCCGGAGTCTGTTCACTACCTT
Alkaline phosphatase	GGGACTGGTACTCGGATAACGA	CTGATATGCGATGTCCTTGCA
Bone sialoprotein	TCCTCCTCTGAAACGGTTTCC	GGAACTATCGCCGTCTCCATT
Cbfa-1	GCCACACTTTCCACACTCTC	CACTTCTGCTTCTTCGTTCTC
GAPDH	CGATGCTGGCGCTGAGTAC	CGTTCAGCTCAGGGATGACC

3. Results

3.1. Substrates

AFM and SEM images showed that the nanotextured substrates were replicated on the PS and the silicone rubber. The nanogrooves on the final silicone rubber surface were smaller and less rectangular than the original template, due to the double replication process. Still, analysis showed constant quality and uniform nanogrooved patterns. The exact sizes of the grooved patterns are shown in Fig. 2. The micropatterned substrates were copied from previous studies [26].

3.2. Image analyses and cell alignment

On the smooth non-stretched surface, cells showed multipolar shapes with no evident distribution in orientation. On all textured non-stretched substrates, an elongated cell shape was seen in parallel direction towards the nanogrooves. When stretch of various magnitude was applied in the cell alignment study, cells changed their initial morphology and direction in both situations (Fig. 3). The quantified results for the cell alignment are presented in the Box–Whisker plots in Fig. 4. Such a graph shows the cell distribution midpoint (median), the first and third quartile (boxes), and the largest and smallest observation (whiskers). The effects of the main parameters are expressed as an alignment percentage of the total number of cells.

Results on the smooth surface showed that the adjustment of cellular alignment depended on the stretch magnitude. The median angle for the cells cultured on the smooth surface was 44.5°. When subjected to mechanical loading, cells gradually aligned in perpendicular direction to the stretch direction (Fig. 4a). The complete cell reorientation was determined by the 8% maximum stretch applied.

On the nanotexured surface cells aligned in parallel direction to the texture with median angle of 16.8°. Notably, a significant cell turnover was initiated when stretch magnitude of over 3% was applied (Fig. 4b). An ANOVA and post-hoc Contrast Test showed that the turnover around 3% is statistically significant (3% vs. the lower stretch magnitudes gives a 2-tailed p-value = 0.010; whereas for 3% vs. the higher stretch magnitudes $p = 0.018$). The parallel alignment to the nanotextured substrate was nearly lost when cells were subjected to the highest stretch of 8% magnitude (Fig. 4c). This level was then used to observe cell alignment with SEM, and quantify the gene expression (q-PCR).

An even higher level of parallel cell alignment was observed when a microtextured substrate was used (Fig. 5). However, cells maintained their parallel orientation to the microgrooves when 8% of stretch was applied. The initial median angle slightly changed insignificantly from 8.6° to 13.4° and cells kept their initial parallel alignment towards the microtexture. In contrast the initial median angle changed significantly from 16.7° to 75.4°, when cells were seeded on a nanotextured surface and were subjected to 8% stretch.

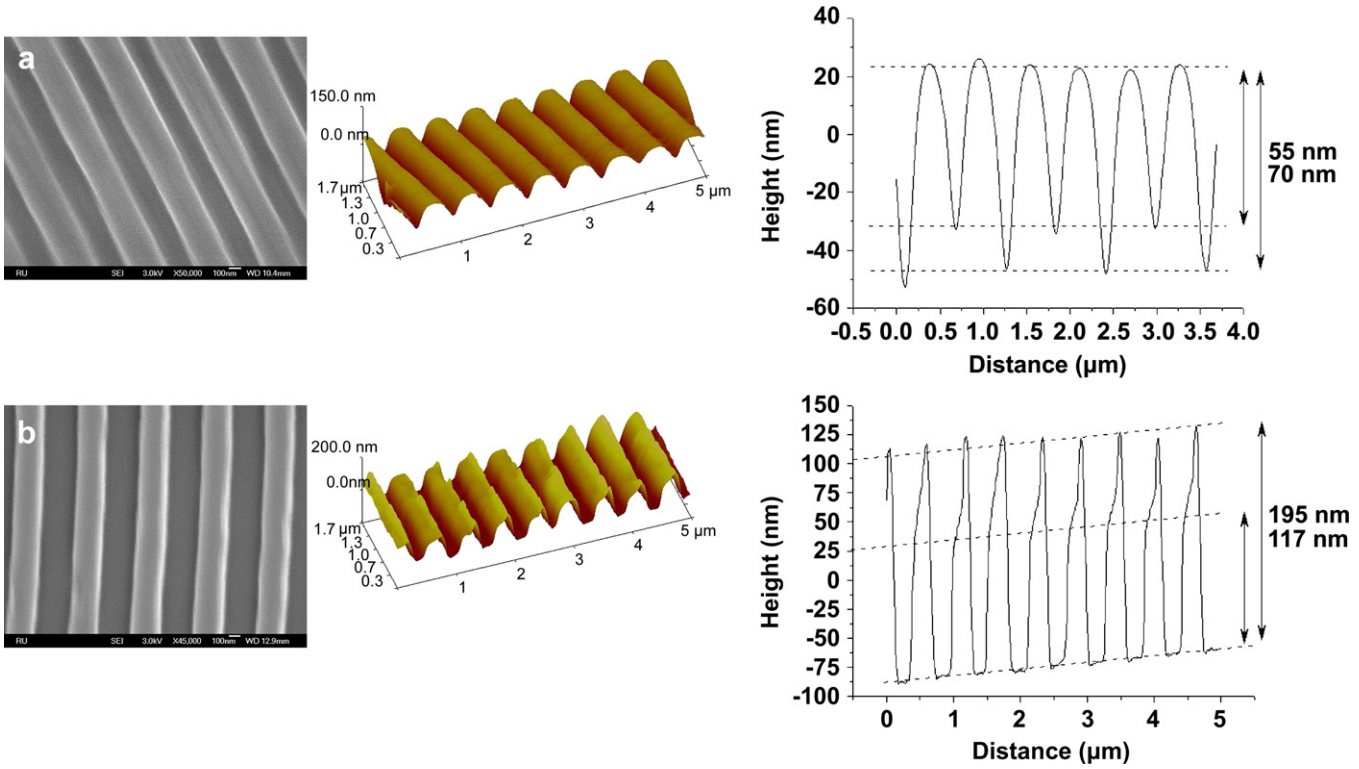

Fig. 2. SEM and AFM graphs of topographies showing height profiles of nanopatterned polystyrene (a) and silicone rubber substrates (b). SEM and AFM confirmed that the pattern of grooves and ridges on the silicone substrate were reproduced with the exact sizes indicated on the graphs. Note that the AFM pattern is deformed due to tip convulsion and only applicable for size measurement.

3.3. Scanning electron microscopy

When analyzing cell morphology, SEM confirmed the orientation analysis and showed that the cells on the smooth substrate spread out in a random fashion and had rounded cell bodies with extensions in multiple directions. When stretch was applied, cells realigned perpendicular to the direction of the applied stretch, while cells adapted elongated bodies. Cells aligned parallel to the

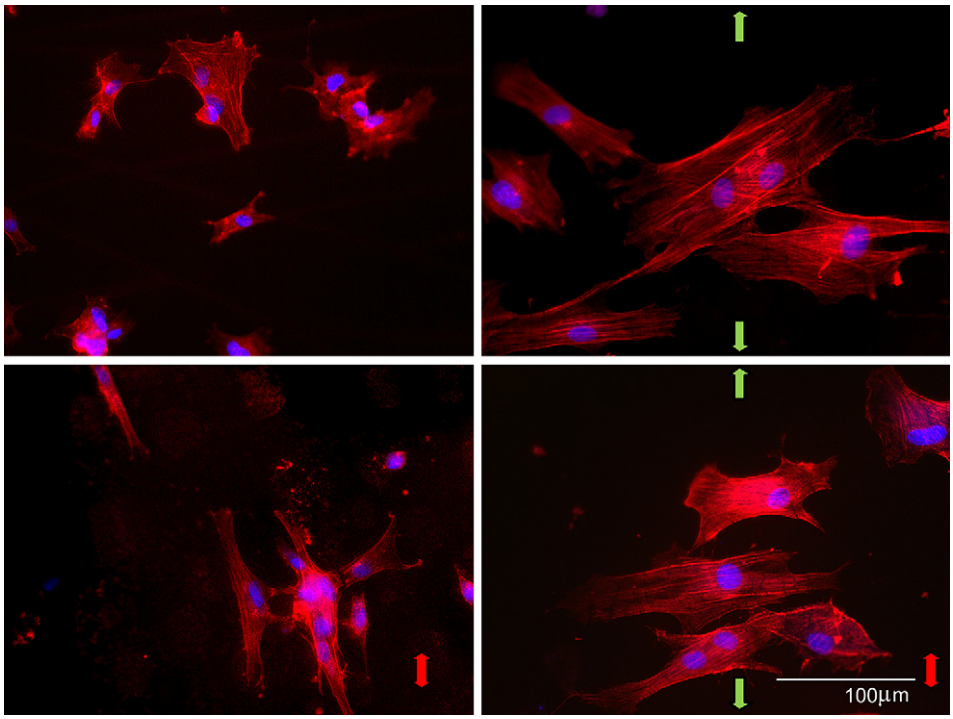

Fig. 3. Fluorescent microscopy micrographs of cellular actin filaments (red) when cultured under several conditions. Top left: random cell orientation, top right: perpendicular cell orientation to the stretch, bottom left: parallel cell orientation to the grooves, bottom right: cell alignment to the substrate nanotexture is lost due to the 8% of stretch. Green and red arrows indicate the direction of the stretch and grooves, respectively.

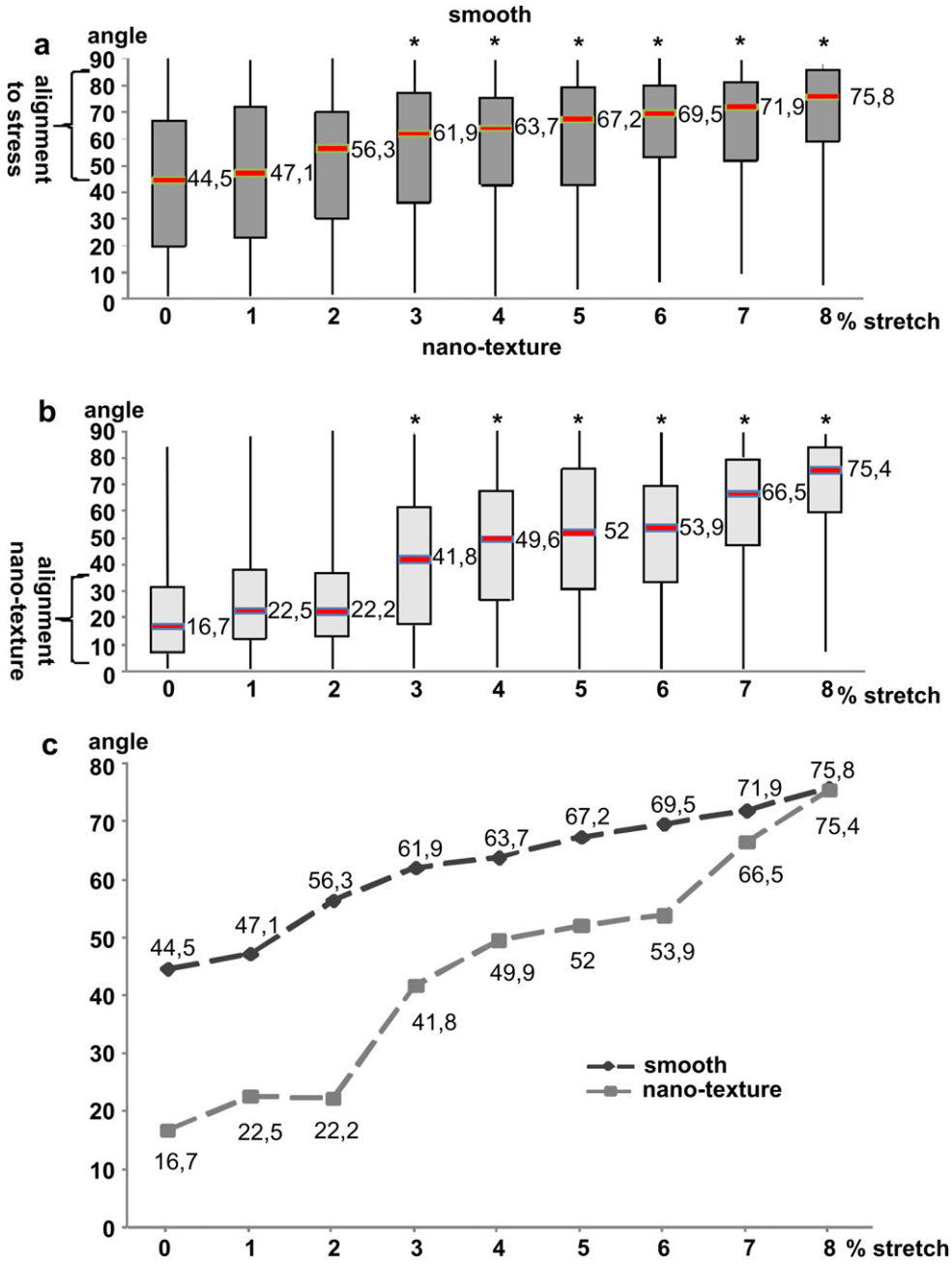

Fig. 4. Box–Whisker plot showing the cellular alignment to the grooves. The median is marked in the box with red and the box-corners indicate the 25–75th percentiles. Median of 45° is a random orientation. (a) Cells subjected to a stretch on a smooth surface showing gradual alignment in perpendicular direction to the stretch force was significally initiated at 3% stretch. The *p*-value in the different groups was calculated against the smooth control. (b) Cells subjected to a stretch on nanotextured surface. The gradual alignment in perpendicular direction to the stretch force was significally initiated at 3% stretch. The *p*-value in the different groups was calculated against the nanotextured surface. (c) Merge of the medians from figures a and b shows that data are converging and effect is maximal when 8% of stretch is applied to the cells. Each box in the plot represents ~ 200 cells (*$p < 0.001$).

grooves when seeded on nanotextured surface and had elongated cell bodies as well. However, the parallel alignment to the nanotextured substrate was lost when cells were subjected to the 8% of stretch, still cells maintained their elongated cell body (Fig. 6).

3.4. Q-PCR

The results from the q-PCR demonstrated large individual differences in between the rats. However, the gene expression was altered in all three conditions when compared to the smooth control. The dual stimulation gave the highest gene expression profile. Statistical analyses confirmed that there is a significant effect (two-way ANOVA, $p < 0.05$) on gene expression for integrin $\alpha 1$, when cells were cultured on the nanotexture. Synergistic effects for combined nanotopography and mechanical stimulation were evident, and let to significant upregulation of gene expression for integrin $\alpha 1$, fibronectin, OC, Cfba and BSP as shown in Fig. 7.

4. Discussion

The idea that the mechanical cell surrounding produces a complex range of biological functions is supported by many

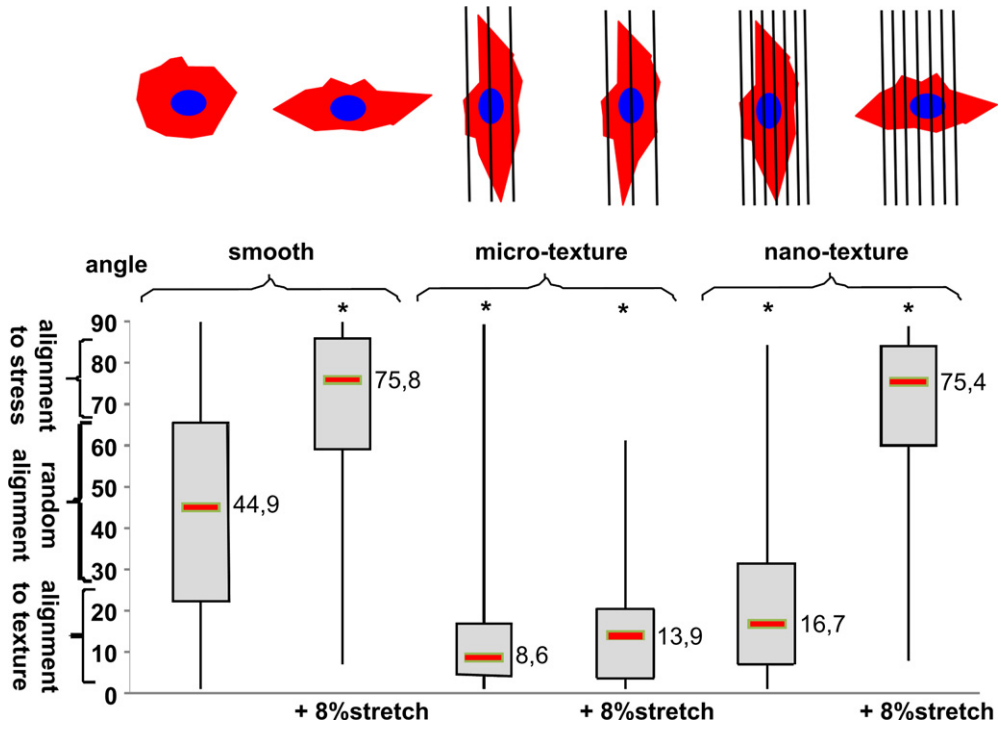

Fig. 5. Box–Whisker plot showing the cellular alignment to the grooves and stretch. Cells align on the microtexture without changes in cell orientation when 8% stretch is applied. Note that cell alignment to the nanotextured substrate is lost due to the stretch force as depicted on the graphs above the plot. The *p*-value in the different groups was calculated against the smooth control ($^*p < 0.001$), and each box in the plot represents ~200 cells.

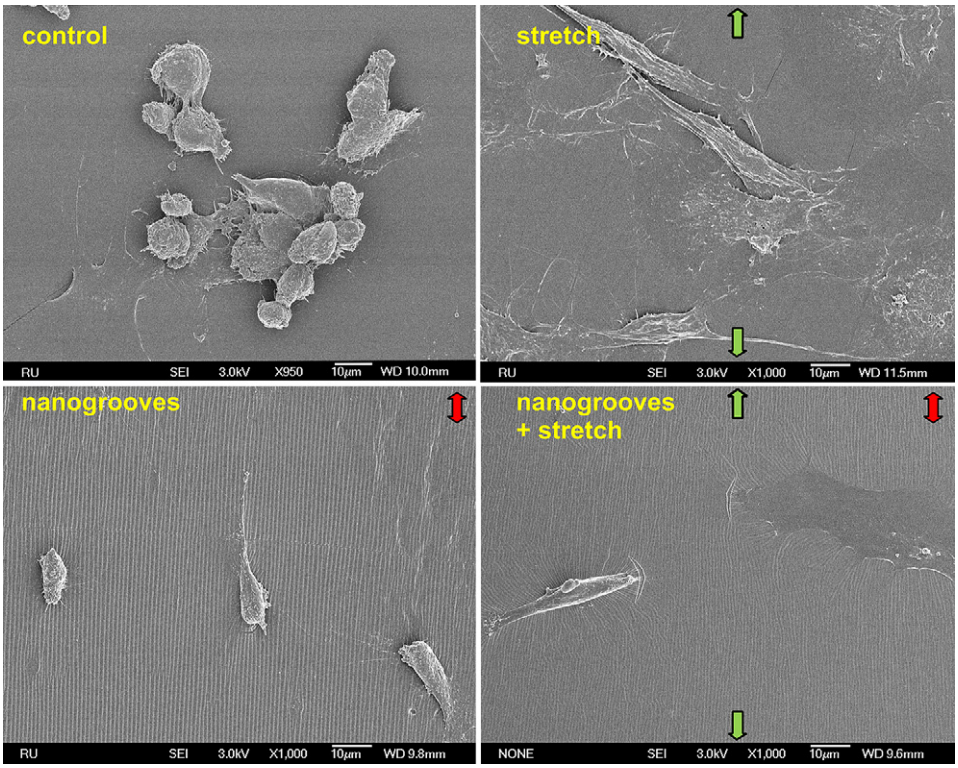

Fig. 6. SEM micrographs of MSCs cultured under various circumstances. Top left: random cell orientation, top right: perpendicular cell orientation to the stretch. Bottom left: parallel cell orientation to the nanogrooves, bottom right: cell alignment to the substrate nanotopography is lost due to the stretch force. However cells retain an elongated phenotype. Green and red arrows indicate the direction of the stretch and grooves, respectively.

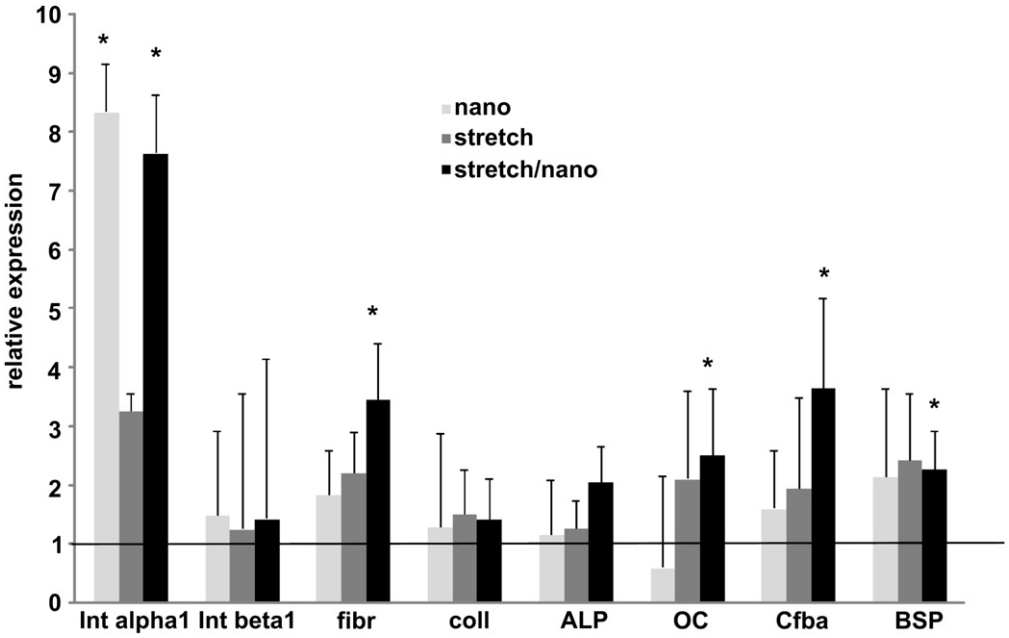

Fig. 7. Influence of nanotexture, stretch, and combination on gene expression evaluated after 2 days of cell-culture stimulation. Values were normalised to GAPDH and relative to the smooth substrates (black line). Statistical analyses confirmed that there is a significant effect (two-way ANOVA, $p < 0.05$) on gene expression for integrin α1 when nanotexture and dual stimulation were used. Significant synergistic effects on gene expression for fibronectin and Cfba were observed when dual stimulation was used (8% of stretch and nanotexture). Note that the dual stimulation gave the highest gene expression profile, $^{*}p < 0.05$, $n = 3$.

recent studies. Cells in the body are embedded in a nanofibrous matrix, and continuously subjected to mechanical strains. Therefore, the aim of this study was to design a multi-factorial model which closely resembles such an environment, and test cell behavior on both structural and biochemical changes in such a model. Experiments were performed to quantify the stretch magnitude-dependence on cell morphological changes. Results showed that morphological adaptation to a nanotextured substrate was completely lost when cells were subjected to the highest stretch magnitude. In addition, a significant synergistic effect on the expression of cell measured genes was achieved when dual stimulation was used.

When regarding our study set-up, the SEM and AFM analysis of the silicone substrates showed that the reproduction of the nanopatterns was not as accurate as previously described for PS. Still, we confirmed that silicone (rubber) surfaces had a constant quality and uniform nanogrooves with a groove width of ~300 nm (pitch 600 nm) and groove depth of ~60 nm. The differences in the depth and the pitch of the silicone rubber replicates compared to original templates are probably due to the high viscosity, and the diffusion limitation of the elastomer in grooves with such small sizes. Furthermore, the capillary forces elicited by the nanogrooves, as-described by van Delft [30], might play a role. Because of these characteristics, we could not produce groove sizes with smaller dimensions in the elastomer, and only vary the rate of mechanical stimulation in our interaction studies. Previous studies showed that the strain fields were homogeneous over the cell culture surface and that the silicone rubber is elastic when small cycle regimes are used [33]. Thus, we did not evaluate the fatigue of the nanotexture after the stretching experiments, because we assumed that small cycle situations and parallel stretch direction to the grooves will not significally damage the nanotexture. As a final technical remark, cells were seeded with lower cell density in the cell alignment studies to better analyze cell morphology, and avoid cell–cell contacts during the image analysis. A higher cell density in the gene expression studies was necessary to obtain sufficient amount of RNA.

To define the exact mechanical stresses acting on bone cells in vivo is difficult, which in term hampers the design of an in vitro models. Various models have been proposed applying different frequencies, stretch magnitudes and durations of mechanical load to examine cell morphology and behavior [34–37]. Our model used constant frequency of 1 Hz, resembling chewing or walking movement and subsequently gradually increased magnitude of stretch from 1% to 8%. Noticeably, on the smooth surface cell alignment improved gradually with increased deformation rates. In contrast deformation-induced loss of alignment on the nanotextures did not occur so gradually. There was a clear preference for the texture-induced cell alignment below 3%, and for the mechanically induced cell shape above 3% of stretch. Further, a complete turnover of cell alignment was observed at stretch magnitude of 8%. Thus, for the subsequent experiments on SEM and gene expression evaluation only 8% stretch was used.

Scanning electron microscopy, immunofluorescence staining, and subsequent image analysis all confirmed that MSCs orient parallel to the nanogrooves. Cells aligned less on grooves with nanodimensions and more on grooves with micro dimensions. This phenomenon was observed earlier in other studies and it is known that an increase in groove dimensions (especially in depth) led to higher cell orientation [26]. It is not fully unraveled how exactly this mechanism works, but certainly cells do not recognise a surface cue anymore when structural dimensions get down to a width of below 75 nm and depth of 33 nm [29]. Integrins, focal adhesions and different cytoskeleton molecules play part in the recognition of surface conformation immediately upon attachment [38]. The mechanism behind mechanical stimulation is believed to be twofold. Direct mechanotransduction relies on the link between the cytoskeleton and nucleus through the nuclear lamins. Cells exposed to stress significantly change shape, upregulate nuclear lamins and move lamins from the nuclear interior to the nuclear periphery, allowing nuclear genomic adaptation to stress [39]. Indirect mechanotransduction is dependent on chemical signaling cascades initiated by focal adhesion-associated proteins [40]. Both signaling pathways together will result in the cell actively adjusting

its shape in the most force-efficient shape. Once cells have oriented and adapted to the new environment, cells remain dependent on the systems to maintain their position, or readjust when new environmental cues arise. In our study, the interaction between the substrate and mechanical environment gave a significant effect in terms of gene expression for ECM formation (fibronectin) and early osteoblasts differentiation (Cfba) when dual stimulation (i.e. combined stretch and nanotexture) was used. The activation of these mechano–physiological signaling events indicates that cells indeed are able to adjust to the mechanical environment in order to maintain biochemical homeostasis.

5. Conclusion

We maintained our hypothesis that nanotexture surface topography and mechanical stimuli can truly interact, and we showed this in multi-factorial model. The parallel cell direction to the nanotextured surface was lost and turned into perpendicular when parallel stretch to the cells was applied. This phenomenon cannot be achieved when a micrometer-sized texture is used. Furthermore, a significant synergistic effect in terms of gene expression for fibronectin and Cfba was observed when dual stimulation was used. These findings can lead to a development of new biomimetic materials that can guide morphogenesis in tissue repair and bone remodeling.

Acknowledgements

We thank Dr. E.M. Bronkhorst for statistical analyses. This study was supported by the Microgravity Research Program of NWO-Space Research Organization Netherlands (SRON, Grant ALW-GO-MG 07-01 and MG-057), the Dutch Technology Foundation STW, applied science division of NWO, Technology Program of the Ministry of Economic Affairs (project 07621) and NanoNed, the Dutch nanotechnology program.

Appendix

Figures with essential colour discrimination. Figs. 1–6 in this article have parts that are difficult to interpret in black and white. The full colour images can be found in the on-line version, at doi:10.1016/j.biomaterials.2010.06.050.

References

[1] Judex S, Gupta S, Rubin C. Regulation of mechanical signals in bone. Orthod Craniofac Res 2009;12(2):94–104.
[2] Sikavitsas VI, Temenoff JS, Mikos AG. Biomaterials and bone mechano-transduction. Biomaterials 2001;22(19):2581–93.
[3] Knothe Tate ML, Steck R, Anderson EJ. Bone as an inspiration for a novel class of mechanoactive materials. Biomaterials 2009;30(2):133–40.
[4] Wang QG, Nguyen B, Thomas CR, Zhang Z, El Haj AJ, Kuiper NJ. Molecular profiling of single cells in response to mechanical force: comparison of chondrocytes, chondrons and encapsulated chondrocytes. Biomaterials;31 (7):1619–25.
[5] Milan JL, Planell JA, Lacroix D. Computational modelling of the mechanical environment of osteogenesis within a polylactic acid-calcium phosphate glass scaffold. Biomaterials 2009;30(25):4219–26.
[6] Carter DR, Van Der Meulen MC, Beaupre GS. Mechanical factors in bone growth and development. Bone 1996;18(Suppl. 1):5S–10S.
[7] Rittweger J. Ten years muscle-bone hypothesis: what have we learned so far? – almost a festschrift. J Musculoskelet Neuronal Interact 2008;8(2):174–8.
[8] Sharp LA, Lee YW, Goldstein AS. Effect of low-frequency pulsatile flow on expression of osteoblastic genes by bone marrow stromal cells. Ann Biomed Eng 2009;37(3):445–53.
[9] Santos A, Bakker AD, Zandieh-Doulabi B, Semeins CM, Klein-Nulend J. Pulsating fluid flow modulates gene expression of proteins involved in Wnt signaling pathways in osteocytes. J Orthop Res 2009;27(10):1280–7.
[10] Vico L, Lafage-Proust MH, Alexandre C. Effects of gravitational changes on the bone system in vitro and in vivo. Bone 1998;22(Suppl. 5):95S–100S.
[11] Van Loon JJ, Bervoets DJ, Burger EH, Dieudonne SC, Hagen JW, Semeins CM, et al. Decreased mineralization and increased calcium release in isolated fetal mouse long bones under near weightlessness. J Bone Miner Res 1995;10 (4):550–7.
[12] Van Loon JJ, van Laar MC, Korterik JP, Segerink FB, Wubbels RJ, de Jong HA, et al. An atomic force microscope operating at hypergravity for in situ measurement of cellular mechano-response. J Microsc 2009;233(2):234–43.
[13] Yeni YN, Dong XN, Fyhrie DP, Les CM. The dependence between the strength and stiffness of cancellous and cortical bone tissue for tension and compression: extension of a unifying principle. Biomed Mater Eng 2004;14 (3):303–10.
[14] Chau JF, Leong WF, Li B. Signaling pathways governing osteoblast proliferation, differentiation and function. Histol Histopathol 2009;24(12):1593–606.
[15] Dumas V, Perrier A, Malaval L, Laroche N, Guignandon A, Vico L, et al. The effect of dual frequency cyclic compression on matrix deposition by osteoblast-like cells grown in 3D scaffolds and on modulation of VEGF variant expression. Biomaterials 2009 Jul;30(19):3279–88.
[16] Song G, Ju Y, Shen X, Luo Q, Shi Y, Qin J. Mechanical stretch promotes proliferation of rat bone marrow mesenchymal stem cells. Colloids Surf B Biointerfaces 2007;58(2):271–7.
[17] Siebers MC, Walboomers XF, van den Dolder J, Leeuwenburgh SC, Wolke JG, Jansen JA. The behavior of osteoblast-like cells on various substrates with functional blocking of integrin-beta1 and integrin-beta3. J Mater Sci Mater Med 2008;19(2):861–8.
[18] Liu W, Toyosawa S, Furuichi T, Kanatani N, Yoshida C, Liu Y, et al. Over-expression of Cbfa1 in osteoblasts inhibits osteoblast maturation and causes osteopenia with multiple fractures. J Cell Biol 2001;155(1):157–66.
[19] Bikle DD. Integrins, insulin like growth factors, and the skeletal response to load. Osteoporos Int 2008;19(9):1237–46.
[20] Takahashi I, Onodera K, Sasano Y, Mizoguchi I, Bae JW, Mitani H, et al. Effect of stretching on gene expression of beta1 integrin and focal adhesion kinase and on chondrogenesis through cell–extracellular matrix interactions. Eur J Cell Biol 2003;82(4):182–92.
[21] Winter LC, Walboomers XF, Bumgardner JD, Jansen JA. Intermittent versus continuous stretching effects on osteoblast-like cells in vitro. J Biomed Mater Res A 2003;67(4):1269–75.
[22] Lenhert S, Meier MB, Meyer U, Chi L, Wiesmann HP. Osteoblast alignment, elongation and migration on grooved polystyrene surfaces patterned by Langmuir–Blodgett lithography. Biomaterials 2005;26(5):563–70.
[23] Meyle J, Wolburg H, von Recum AF. Surface micromorphology and cellular interactions. J Biomater Appl 1993;7(4):362–74.
[24] Charest JL, Bryant LE, Garcia AJ, King WP. Hot embossing for micropatterned cell substrates. Biomaterials 2004;25(19):4767–75.
[25] Matsuzaka K, Walboomers XF, Yoshinari M, Inoue T, Jansen JA. The attachment and growth behavior of osteoblast-like cells on microtextured surfaces. Biomaterials 2003;24(16):2711–9.
[26] Loesberg WA, Walboomers XF, van Loon JJ, Jansen JA. The effect of combined cyclic mechanical stretching and microgrooved surface topography on the behavior of fibroblasts. J Biomed Mater Res A 2005;75(3):723–32.
[27] Shaub A. Unravelling the extracellular matrix. Nat Cell Biol 1999;1(7):E173–5.
[28] Walboomers XF, Croes HJ, Ginsel LA, Jansen JA. Growth behavior of fibroblasts on microgrooved polystyrene. Biomaterials 1998;19(20):1861–8.
[29] Lamers E, Walboomers XF, Domanski M, te Riet J, van Delft FC, Luttge R, et al. The influence of nanoscale grooved substrates on osteoblast behavior and extracellular matrix deposition. Biomaterials 2010;31(12):3307–16.
[30] van Delft F, van den Heuvel FC, Loesberg WA, te Riet J, Schön P, Figdor CG, et al. Manufacturing substrate nano-grooves for studying cell alignment and adhesion. Microelectron Eng 2008;85(5–6):1362–6.
[31] Neidlinger-Wilke C, Grood ES, Wang J-C, Brand RA, Claes L. Cell alignment is induced by cyclic changes in cell length: studies of cells grown in cyclically stretched substrates. J Orthop Res 2001;19(2):286–93.
[32] Maniatopoulos C, Sodek J, Melcher AH. Bone formation in vitro by stromal cells obtained from bone marrow of young adult rats. Cell Tissue Res 1988;254(2):317–30.
[33] Neidlinger-Wilke C, Wilke HJ, Claes L. Cyclic stretching of human osteoblasts affects proliferation and metabolism: a new experimental method and its application. J Orthop Res 1994;12(1):70–8.
[34] Hsu HJ, Lee CF, Kaunas R. A dynamic stochastic model of frequency-dependent stress fiber alignment induced by cyclic stretch. PLoS One 2009;4(3):e4853.
[35] Garman R, Rubin C, Judex S. Small oscillatory accelerations, independent of matrix deformations, increase osteoblast activity and enhance bone morphology. PLoS One 2007;2(7):e653.
[36] Ozcivici E, Garman R, Judex S. High-frequency oscillatory motions enhance the simulated mechanical properties of non-weight bearing trabecular bone. J Biomech 2007;40(15):3404–11.
[37] Deng D, Liu W, Xu F, Yang Y, Zhou G, Zhang WJ, et al. Engineering human neo-tendon tissue in vitro with human dermal fibroblasts under static mechanical strain. Biomaterials 2009;30(35):6724–30.
[38] Walboomers XF, Ginsel LA, Jansen JA. Early spreading events of fibroblasts on microgrooved substrates. J Biomed Mater Res 2000;51(3):529–34.
[39] Philip JT, Dahl KN. Nuclear mechanotransduction: response of the lamina to extracellular stress with implications in aging. J Biomech 2008;41 (15):3164–70.
[40] Dalby MJ, Yarwood SJ. Analysis of focal adhesions and cytoskeleton by custom microarray. Methods Mol Biol 2007;370:121–34.